Analysis of Site-Specific Histidine Protonation in Human Prolactin[†,‡]

M. Cristina Tettamanzi, Camille Keeler, Syrus Meshack, and Michael E. Hodsdon*

Department of Laboratory Medicine, Yale University, New Haven, Connecticut 06520

Received March 14, 2008; Revised Manuscript Received May 29, 2008

ABSTRACT: The structural and functional properties of human prolactin (hPRL), a 23 kDa protein hormone and cytokine, are pH-dependent. The dissociation rate constant for binding to the extracellular domain of the hPRL receptor increases nearly 500-fold over the relatively narrow and physiologic range from pH 8 to 6. As the apparent midpoint for this transition occurs around pH 6.5, we have looked toward histidine residues as a potential biophysical origin of the behavior. hPRL has a surprising number of nine histidines, nearly all of which are present on the protein surface. Using NMR spectroscopy, we have monitored site-specific proton binding to eight of these nine residues and derived equilibrium dissociation constants. During this analysis, a thermodynamic interaction between a localized triplet of three histidines (H27, H30, and H180) became apparent, which was subsequently confirmed by site-directed mutagenesis. After consideration of multiple potential models, we present statistical support for the existence of two negative cooperativity constants, one linking protonation of residues H30 and H180 with a magnitude of approximately 0.1 and the other weaker interaction between residues H27 and H30. Additionally, mutation of any of these three histidines to alanine stabilizes the folded protein relative to the chemically denatured state. A detailed understanding of these complex protonation reactions will aid in elucidating the biophysical mechanism of pH-dependent regulation of hPRL's structural and functional properties.

Prolactin (PRL) is a 23 kDa protein hormone and a member of the family of hematopoietic cytokines, which includes erythropoietin, granulocyte colony-stimulating factor, interleukin-6, and many others, but is most closely related both evolutionarily and functionally to human growth hormone (hGH)[1] and placental lactogen (hPL) (*1*). Proteins in this family share a common four-α-helical bundle structural topology and recognize a conserved family of type 1 cytokine receptors (*2*). In humans, PRL is secreted by pituitary lactotrophs under hypothalamic regulation, where it circulates in the bloodstream and acts distally as an endocrine hormone. Human PRL (hPRL)[1] is also synthesized in many extrapituitary tissues, including breast, prostate, and the female reproductive tract, where it appears to act locally to regulate cellular growth and differentiation (*3, 4*). Closely associated with this autocrine/paracrine function as a local growth factor or cytokine, hPRL has been implicated in the growth and development of human cancers arising from the same tissue sites (*5–8*). Interestingly, a number of post-translational modifications to PRL have been identified, including phosphorylated (*9–13*) and proteolytically cleaved (*14–17*) variants, which appear to largely counter the protumorigenic activities of the wild-type (WT) hormone.

We recently described a dependence of the structural and functional properties of hPRL on solution pH (*18*). The structural stability of the recombinant protein decreases from 7.6 kcal/mol at pH 8 to 5.6 kcal/mol at pH 6. More striking is the greater than 500-fold decrease in the equilibrium association constant for the extracellular domain of the PRL receptor over this same relatively narrow and physiologic pH range. The biologic consequences of these effects are currently undescribed, but many possibilities exist. A pH-dependent conformational change and subsequent aggregation reaction have been postulated to drive packaging of the newly expressed hormone into the secretory granules of pituitary lactotrophs (*19, 20*). The mechanisms for generating the phosphorylated and proteolytically cleaved variants of hPRL are not well understood but could be regulated by pH-dependent destabilization of the protein. Proteolytic cleavage of hPRL by the endocytic enzyme cathepsin D has been proposed (*21, 25*). As cathepsin D is activated by acidic environments around pH 5−6, perhaps concomitant structural destabilization of hPRL increases its susceptibility to proteolytic cleavage in a synergistic manner. Similarly, as phosphorylation of hPRL at S179 is complicated by the complete burial of its side chain within the helical bundle, acid-induced destabilization of the protein may allow phosphorylating enzymes access to the residue. Lastly, the biology of hPRL must be impacted by the dramatic decrease in receptor binding affinity occurring between the physiologic pH range of 7.3−7.5 and slightly more acidic values between

[†] This work was supported by National Institutes of Health Grant R01 CA108992.

[‡] Chemical shift data have been deposited in BioMagResBank (BMRB) as entry 15773.

* To whom correspondence should be addressed: P.O. Box 208035, Department of Laboratory Medicine, Yale University, New Haven, CT 06520-8035. Telephone: (203) 737-2674. Fax: (203) 688-8704. E-mail: michael.hodsdon@yale.edu.

[1] Abbreviations: hPRL, human prolactin; hGH, human growth hormone; hPL, human placental lactogen; WT, wild type; NMR, nuclear magnetic resonance; DSS, 2,2-dimethyl-2-silapentane-5-sulfonate, sodium salt; HSQC, heteronuclear single-quantum coherence; 2D, two-dimensional; INEPT, insensitive nuclei enhanced (by) polarization transfer; SSE, sum-squared error; IPTG, isopropyl β-D-1-thiogalactopyranoside; PMSF, phenylmethanesulfonyl fluoride; GARP, globally optimized alternating phase rectangular pulse.

10.1021/bi800444t CCC: $40.75
Published on Web 07/25/2008

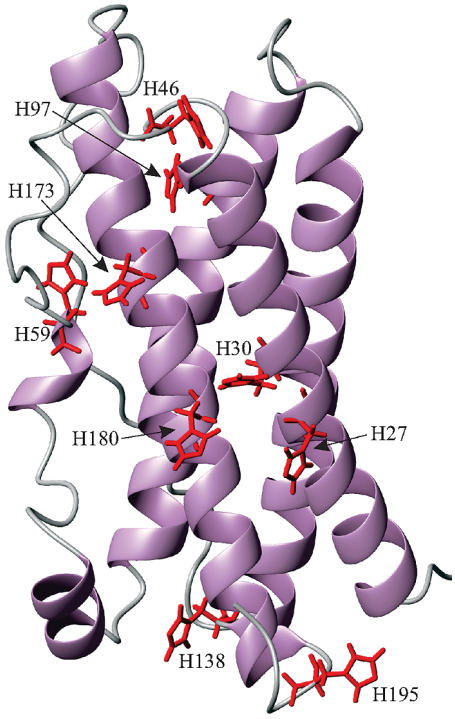

FIGURE 1: Backbone ribbon diagram for the tertiary structure of hPRL [Protein Data Bank (PDB) entry 1RW5, first member of the ensemble shown] with histidine side chains highlighted in red and labeled with their respective residue number.

6.0 and 6.5. A similar shift in pH can be seen in the extracellular fluid of malignant versus surrounding tissues (*26*), implying decreased receptor occupancy of hPRL in hypoxic tumors. Also, after endocytosis of hPRL−receptor complexes, the subsequent decrease in endosomal pH should induce dissociation of the hormone from the receptor.

We have begun to explore the biophysical basis for the pH-dependent regulation of the structural and functional properties of hPRL described above. As the observed perturbations occur largely over a pH range from 6 to 8, with an apparent midpoint to the transition around pH 6.5, protonation of the imidazole side chains of His residues is the most likely origin of the behavior. hPRL contains a surprising number of nine histidines, comprising 4.5% of its amino acids, in comparison to the lower 2% incidence of histidines in a survey of modern proteins (*27*). The closely related proteins hGH and hPL contain three and seven His residues, respectively. Displayed on the tertiary structure of hPRL (*28, 29*) in Figure 1, His imidazoles are largely dispersed throughout the protein surface, with the exception of a single localized cluster of H27, H30, and H180, which forms part of the expected high-affinity receptor binding site (*29*). To improve our understanding of the protonation reactions occurring in hPRL around pH 6.5, we have measured site-specific pH titrations for each of the observable histidines using NMR spectroscopy under near-physiologic solution conditions. Although a majority of His residues titrated according to a classic "Henderson−Hasselbach" model, the localized triplet of H27, H30, and H180 displayed more complex behavior. Given the likely importance of these residues in regulating pH-dependent receptor binding, a detailed analysis of their protonation reactions is warranted and presented here.

EXPERIMENTAL PROCEDURES

Preparation of Isotope-Labeled Recombinant Proteins for NMR Spectroscopy. Wild-type (WT) human prolactin (hPRL) was recombinantly expressed in BL21 DE3 *Escherichia coli* and purified from inclusion bodies as previously described (*30*). Expression vectors for the H27A, H30A, and H180A hPRL site-directed mutants of hPRL were obtained from C. Clevenger (Northwestern University, Evanston, IL), and protein was similarly prepared. Uniform ^{13}C and ^{15}N protein labeling was achieved using growth in M9 minimal medium, appropriately enriched with 1 g of [^{15}N]NH_4Cl and 3 g of [U-$^{13}C_6$]glucose (Cambridge Isotope Laboratories, Inc., Andover, MA) per liter of bacterial culture. Selective [^{15}N]histidine-labeled WT and H180A hPRL were prepared by transformation of their expression vectors into a histidine auxotroph strain of BL21(DE3) *E. coli* developed (*31*) and generously provided by D. Waugh (National Cancer Institute, Bethesda, MD). Similar M9 minimal medium was supplemented with [^{15}N]histidine (Cambridge Isotope Laboratories, Inc.) and all other unlabeled amino acids (Sigma-Aldrich, Inc., St. Louis, MO) on the basis of a previous protocol (*32*). After transformation, the auxotrophic bacteria were plated onto LB-enriched agar containing 0.2 g/L ampicillin and incubated overnight at 37 °C. A single isolated colony was used to inoculate 50 mL of the minimal medium, also with 0.2 g/L ampicillin, and again incubated overnight at 37 °C. An aliquot of this culture was used to inoculate 1 L of minimal medium supplemented with 0.1 g of each unlabeled amino acid and 0.02 g of unlabeled histidine. After growth of this culture at 37 °C until its absorbance at 600 nm reached ~0.8, 0.1 g of [^{15}N]histidine was added and allowed to grow for an additional 10 min before induction of recombinant protein expression by the addition of IPTG to a final concentration of 200 mM. Finally, [^{15}N]histidine-labeled hPRL was refolded and purified from inclusion bodies as described above with yields between 50 and 100 mg of purified protein.

For NMR spectroscopy, hPRL was concentrated to 0.6 mM (unless otherwise noted) and exchanged into 25 mM potassium phosphate buffer (pH 7.5), 25 mM NaCl, 5% ^2H_2O, 1 mM NaN_3, and the protease inhibitors leupeptin, pepstatin, and PMSF (1 μM each). A series of samples at different pH values, typically within a range of 4−8, were prepared for ^{13}C- and ^{15}N-enriched WT, H27A, H30A, H173A, and H180A hPRL and for [^{15}N]histidine-labeled WT and H180A hPRL. The samples were put in susceptibility-matched NMR tubes (Shigemi, Inc., Allison Park, PA) for low-volume samples, and the pH was adjusted to the desired values with 10−50 μL of 0.1 M HCl or 0.1 M NaOH. The pH adjustment was performed by adding HCl or NaOH drop by drop, waiting 2 min after each addition to let the pH reach equilibrium. Special care was taken in the preparation of lower-pH samples to prevent protein precipitation, and the sample was centrifuged if precipitation did occur. The resulting pH of each sample was determined at room temperature before and after NMR data collection. The pH was measured in the NMR tube with a model 9826BN Orion glass micro-pH meter combination electrode (Ag/AgCl) (Thermo Electron Corp., Waltham, MA) using an Accumet AP61 pH meter (Fisher Scientific, Pittsburgh, PA).

NMR Spectroscopy. All NMR experiments were conducted on a Varian INOVA 600 MHz spectrometer using a 5 mm triple-resonance probe equipped with triple-axis pulsed magnetic field gradients and utilized pulse sequences from the Varian BioPack User Library (Varian Inc., Palo Alto, CA). Histidine side chain resonance assignments were determined using ^{1}H−^{13}C HSQC and ^{1}H−^{15}N HSQC NMR experiments conducted at 35 °C. The ^{1}H−^{13}C HSQC spectra were recorded with a spectral width of 9000.9 Hz and 2048 total (real plus imaginary) points in the ^{1}H dimension and a spectral width of 4100 Hz and 256 quadrature (real plus imaginary) increments in the ^{13}C dimension, signal-averaged over 128 transients, and with a relaxation delay of 1 s. For the His-tautomeric ^{1}H−^{15}N HSQC NMR experiments, the BioPack library "gNhsqc" pulse sequence was modified as previously described (*33*) to allow GARP ^{13}C decoupling during the evolution of the ^{15}N chemical shift, and spectra were recorded with a spectral width of 8000 Hz and 1024 total (real plus imaginary) points in the ^{1}H dimension and a spectral width of 2500 Hz and 128 quadrature (real plus imaginary) increments in the ^{15}N dimension, signal-averaged over 256 transients, and with a relaxation delay of 1 s. To detect long-range couplings between imidazole ring ^{15}N nuclei and the $^1H_{\delta1}$ and $^1H_{\varepsilon2}$ nuclei, the INEPT relaxation delay was adjusted to correspond to an effective $^2J_{NH}$ coupling constant of 22 Hz, which represents a compromise between the theoretical value of 5−10 Hz (absolute value) and losses in the signal-to-noise ratio due to transverse (R_2) relaxation (*33*). The spectra were recorded for the WT and mutant hPRL at pH values ranging from 3.97 to 8.30. All NMR spectra were processed using NMRPipe (*34*), with subsequent display and analysis in Sparky (*35*). Chemical shifts were referenced indirectly to external DSS at 0.00 ppm, with heteronuclear dimensions referenced using their relative gyromagnetic ratios (*36*).

Curve Fitting and Statistical Analysis. NMR spectra were recorded at many pH values between pH 4.0 and 8.5 for WT and mutant variants of hPRL. Signs of protein precipitation were noticeable below pH 4.0. Equilibrium thermodynamic parameters were derived for eight of the nine histidines in hPRL from the pH dependencies of their NMR chemical shifts. Using Scientist 3.0 (Micromath Research Inc., St. Louis, MO), the observed, pH-dependent chemical shifts (δ_{obs}) were fitted to a simple linear combination of the fully protonated (δ_{AH^+}) and deprotonated (δ_A) states weighted by their relative populations:

$$\delta_{obs} = \delta_{AH^+} f_{AH^+} + \delta_A f_A \quad (1)$$

For each of the independently titrating residues (H46, H59, H138, H173, and H195)

$$f_{AH^+} = \frac{10^{pK_a - pH}}{1 + 10^{pK_a - pH}} \quad (2)$$

$$f_A = 1 - f_{AH^+} \quad (3)$$

For the triplet of coupled titration sites (H27, H30, and H180) modeled in Figure 2, a binding polynomial (*37*) was written as

$$Z = 1 + K_{27}H + K_{30}H + K_{180}H + K_{27}K_{180}H^2 + c_{27,30}K_{27}K_{30}H^2 + c_{30,180}K_{30}K_{180}H^2 + c_{27,30}c_{30,180}K_{27}K_{30}K_{180}H^3 \quad (4)$$

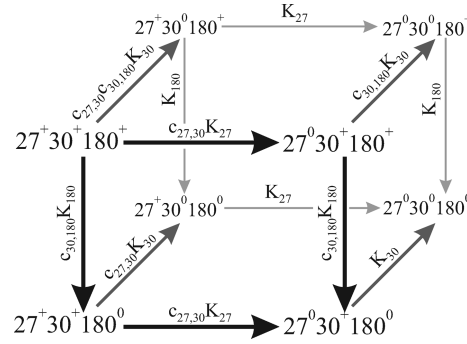

FIGURE 2: Thermodynamic model for protonation of the imidazole rings of H27, H30, and H180 in hPRL, where the superscript denotes the state of each residue. The linkage coefficients and acid dissociation constants describing each deprotonation reaction are shown above their respective arrows.

where $H = 10^{-pH}$ and $K_X = 10^{pK_{a,X}}$. The fractions of protonated and unprotonated states with respect to any single residue, X, were expressed as

$$f_{XH^+} = \frac{d(\ln Z)}{d(\ln K_X)} = \frac{dZ}{dK_X}\frac{K_X}{Z} \quad (5)$$

$$f_X = 1 - f_{XH^+} \quad (6)$$

A variety of possible thermodynamic linkages were considered for the triplet of H27, H30, and H180, detailed in Results. Fixing the two cooperativity constants ($c_{27,30}$ and $c_{30,180}$) at unity during global fitting of the data simulated an independent titration model for these three residues. Alternatively, allowing either or both of the cooperativity constants to float during fitting evaluated possible thermodynamic linkages between either residues H27 and H30 alone, residues H30 and H180 alone, or both pairs of residues simultaneously.

For the statistical analysis presented in Tables 2 and 3 of the Results, F-statistics were calculated as follows:

$$F = \frac{\dfrac{SSE_1 - SSE_2}{P_2 - P_1}}{\dfrac{SSE_2}{n - P_2}} \quad (7)$$

where SSE_1 and SSE_2 represent the sum-squared errors (or residuals) between the experimental data and their best fit values for the two models under comparison. The more simplistic model 1 was considered nested within (or a special case of) the more complex model 2. The number of fitting parameters for each model was represented by P_2 and P_1, where P_2 must be greater than P_1, and n was the number of independent experimental data points used to fit both models. Note that by definition the more complex model provides a better fit to the data (i.e., $SSE_1 > SSE_2$), and the F-statistic tests whether this improvement in the fit was statistically significant by comparison to corresponding "critical" values derived from the F-distribution, based on a desired probability threshold and the appropriate degrees of freedom in the comparison, in this case, $P_2 - P_1$ and $n - P_2$. Threshold probability values in Table 3 for each calculated F-statistic were calculated in Excel (Microsoft Corp., Seattle, WA) using the FDIST command.

Monitoring Urea Unfolding of hPRL Using Intrinsic Trp Fluorescence. A 9.8 M urea (ultrapure) (American Bioanalytical, Natick, MA) stock solution was prepared and its

Table 1: Summary of Fitting the $^1H_{\varepsilon 1}$ NMR Chemical Shifts for the Triplet of H27, H30, and H180 According to the Model of Linked Protonation Sites in Figure 2

model	H27 pK_a	H30 pK_a	H180 pK_a	$c_{27,30}$	$c_{30,180}$
(1) all independent	6.58 (6.36−6.80)	5.28 (5.06−5.51)	5.86 (5.67−6.05)	1 (fixed)	1 (fixed)
(2) H27−H30 interaction	6.66 (6.48−6.84)	6.10 (5.87−6.34)	5.85 (5.73−6.00)	0.07 (0.02−0.13)	1 (fixed)
(3) H30−H180 interaction	6.58 (6.45−6.71)	5.70 (5.54−5.85)	5.96 (5.82−6.10)	1 (fixed)	0.10 (0.01−0.20)
(4) H27−H30 and H30−H180 interactions	6.64 (6.49−6.79)	6.00 (5.67−6.33)	5.96 (5.83−6.09)	0.42 (0.03−0.82)	0.14 (0.02−0.27)

Table 2: Summary of the Sum-Squared Errors (SSEs) and Corresponding Statistical Parameters for Each of the Binding Models Considered[a]

	(1) independent	(2) $c_{27,30}$	(3) $c_{30,180}$	(4) $c_{27,30}$ and $c_{30,180}$	N (data points)
H27 $^1H_{\varepsilon 1}$ SSEs	0.024742	0.008757	0.024742	0.016949	34
H30 $^1H_{\varepsilon 1}$ SSEs	0.087695	0.014108	0.015538	0.012907	34
H180 $^1H_{\varepsilon 1}$ SSEs	0.058582	0.058582	0.014959	0.018397	34
total SSEs	0.17102	0.081448	0.05524	0.048253	102
no. of parameters	9	10	10	11	

[a] SSEs are separately calculated for each independent variable along with the total error.

concentration confirmed from refractive index measurements using a model R5000 hand-held refractometer (Atago U.S.A., Bellevue, WA). A series of 24 buffered urea solutions were prepared in quadruplicate in a 96 deep-well tray using an automated reagent dispenser (Thermo Electron Corp., model Multidrop DW) controlled via the serial port of a personal computer. All urea solutions contained 25 mM NaCl and were buffered to their reported pH with 25 mM potassium phosphate buffer. All pH measurements were taken with an Accumet AP61 hand-held pH meter (Fisher Scientific) and a model 9826BN Orion glass micro-pH combination electrode (Ag/AgCl) (Thermo Electron Corp.). Protein solutions were manually transferred into the deep-well plates containing the buffered urea solutions using a multichannel pipet to a typical final concentration of 6 μM, after which the deep-well plates were sealed with adhesive aluminum film, manually tumbled to stir, and allowed to equilibrate for a minimum of 2 h at room temperature (23 °C) prior to fluorescence readings. Protein/urea solutions were manually transferred to quartz cuvettes in a Cary Eclipse fluorescence spectrophotometer (Varian Instruments, Walnut Creek, CA) employing both temperature control and stirring with micro stir bars. Fluorescence measurements were carried out with an excitation wavelength of 280 nm with a 20 nm slit width and detection at 325 nm with a 5 nm slit width.

RESULTS

Assignment of Histidine Imidazole Ring Chemical Shifts. $^1H-^{13}C$ HSQC and $^1H-^{15}N$ HSQC spectra of uniformly ^{13}C- and ^{15}N-labeled and [^{15}N]His-labeled hPRL recorded at several pH values provided the data for the titration curves of the ^1H, ^{13}C, and ^{15}N nuclei in the histidine imidazole rings. The assignment of each histidine $^1H(^{13}C)_\varepsilon$ imidazole chemical shifts signal in the $^1H-^{13}C$ HSQC spectra was achieved using uniformly ^{13}C- and ^{15}N-labeled His to Ala hPRL mutants and preexisting assignments available in the BMRB (entries 5599 and 6643). These $^1H_\varepsilon$ chemical shift values from $^1H-^{13}C$ HSQC spectra allow us to assign unequivocally the $^{15}N_\varepsilon$, $^{15}N_\delta$, and $^1H_\delta$ histidine chemical shifts in the $^1H-^{15}N$ HSQC hPRL spectra. The assigned chemical shifts are given as Supporting Information and also have been deposited in the BioMagResBank (entry 15773).

Identification of the Histidine Tautomeric States. Previous investigators have recognized how histidine side chains have distinctive ^{15}N NMR chemical shifts depending on the protonation state of the imidazole ring (*33, 38*). In the neutral state, the unprotonated nitrogen is located at higher NMR chemical shifts (up to 80 ppm) compared to its protonated counterpart. As the neutral imidazole ring becomes protonated with a lowering of solution pH, the chemical shift of the originally unprotonated nitrogen migrates to progressively lower values. Figure 3 displays how these differences in chemical shifts, along with the relative intensities of the $^2J_{NH}$-coupled $^{15}N_{\delta 1}-^1H_{\varepsilon 1}$ and $^{15}N_{\varepsilon 2}-^1H_{\delta 2}$ cross-peaks in a $^1H-^{15}N$ HSQC NMR spectrum, allow the identification of the His tautomeric state and correct chemical shift assignment of these four nuclei. In a neutral imidazole ring, depending on the location of the nitrogen-bonded hydrogen, two tautomeric states are possible. The most common tautomeric state ($N_{\varepsilon 2}$-H) has a pattern as shown in the top left portion of Figure 3. $^1H_{\varepsilon 1}$ correlates with two ^{15}N frequencies, one at ~167.5 ppm corresponding to the protonated nitrogen and one at ~249.5 ppm corresponding to the unprotonated nitrogen. $^1H_{\delta 2}$ correlates only with a nitrogen frequency corresponding to one protonated nitrogen as the $^3J(^{15}N_{\delta 1}-^1H_{\delta 2})$ coupling is too small (1−2 Hz) to result in an observable cross-peak. This pattern enables the unambiguous assignment of the nuclei and at the same time specifies which nitrogen is protonated. In the less common $N_{\delta 1}$-H tautomeric state shown in the top right portion of Figure 3, $^{15}N_{\delta 1}$ is protonated and the $^{15}N_{\varepsilon 2}-^1H_{\delta 2}$ cross-peak is located at 249.5 ppm for the ^{15}N chemical shift.

Shown at the bottom of Figure 3 is the $^1H-^{15}N$ HSQC spectrum collected on [^{15}N]His-labeled WT hPRL at pH 7.5, with individual histidine spin systems noted. By simple inspection of their patterns, we conclude that, at pH 7.5, H27, H46, H59, H173, and H180 are in the more common $N_{\varepsilon 2}$-H tautomeric state, whereas H30 adopts the less common $N_{\delta 1}$-H tautomeric state. Spin systems for H59, H97, H138, and H195 were either missing or incomplete, precluding assignment of their tautomeric states. Although the $^1H_{\delta 2}$ and $^1H_{\varepsilon 1}$ nuclei detected in this experiment do not undergo rapid exchange with solvent, they are susceptible to line broadening from rapid amide hydrogen exchange elsewhere in the imidazole ring or potential conformational exchange processes, which we presume are responsible for the missing resonances. Finally, Figure 4 shows superposed $^1H-^{15}N$ HSQC spectra of [^{15}N]His-labeled WT hPRL ranging from pH 4.5 to 8.0. The changes in ^1H and ^{15}N chemical shifts versus pH are generally linear, consistent with perturbations due to only a single pH-dependent reaction, with the dramatic exception of the $^{15}N_{\delta 1}$ nucleus of H30. In the spectral expansion shown for WT hPRL, the H30 $^1H_{\varepsilon 1}-^{15}N_{\delta 1}$ cross-peak follows a highly curved trajectory, indicating a dependence on more than one pH-dependent effect. We hypothesize that, given the close relationship between the H30 and

Table 3: *F*-Statistic Calculations Comparing Each Binding Model with Corresponding Probability Values in Parentheses[a]

	(2) H27−H30 interaction	(3) H30−H180 interaction	(4) H27−H30 and H30−H180 interactions
	H27 $H_{\varepsilon 1}$		
(1) all independent	43.8 (7.6×10^{-7})	equivalent[b]	5.3 (0.013)
(2) H27−H30 interaction			rejected[c]
(3) H30−H180 interaction			10.6 (0.004)
	H180 $H_{\varepsilon 1}$		
(1) all independent	equivalent[b]	70.0 (1.4×10^{-8})	25.2 (1.6×10^{-6})
(2) H27−H30 interaction			50.2 (3.2×10^{-7})
(3) H30−H180 interaction			rejected[c]
	H30 $H_{\varepsilon 1}$		
(1) all independent	125.2 (5.2×10^{-11})	111.5 (1.7×10^{-10})	66.6 (2.7×10^{-10})
(2) H27−H30 interaction			2.1 (0.16)
(3) H30−H180 interaction			4.7 (0.041)
	All Data		
(1) all independent	101.2 (1.7×10^{-16})	192.8 (2.66×10^{-24})	115.8 (9.9×10^{-26})
(2) H27−H30 interaction			62.6 (5.8×10^{-12})
(3) H30−H180 interaction			13.2 (4.7×10^{-4})

[a] The first three boxes represent each individual dependent variable used during fitting, and the last considers all data. [b] No improvement in fit between models. [c] The more complex model has the poorer fit.

H180 imidazole rings in the tertiary structure of hPRL, the H30 $^{15}N_{\delta 1}$ nucleus must detect protonation of both residues approximately equally. This was confirmed by reversion to a linear trajectory in [^{15}N]His-labeled H180A hPRL, which can be seen in the second expansion at the bottom right of Figure 4.

pH-Dependent Titration of His NMR Chemical Shifts for WT, H27A, H30A, H173A, and H180A hPRL. Figure 5 plots the $^{1}H_{\varepsilon 1}$ and $^{13}C_{\varepsilon 1}$ NMR chemical shifts against solution pH for eight of the nine His residues in hPRL. Titrations are superposed for both the WT protein and multiple His to Ala mutants to assess the effect of the mutations on the other residues. Not shown are the analogous pH titration curves for the four additional imidazole ring nuclei (i.e., $^{15}N_{\varepsilon 2}$, $^{15}N_{\delta 1}$, $^{1}H_{\delta 2}$, and $^{1}H_{\varepsilon 2}$), which were also collected for a majority of the residues. The $^{1}H_{\varepsilon 1}$ and $^{13}C_{\varepsilon 1}$ nuclei provided the largest number of data points and the most complete titration curves. For the five residues shown at the top of the figure, there is very good agreement among the titration data across the large number of independent NMR samples, which represent different protein preparations, labeling schemes, and even mutants of hPRL. We compared simultaneous fitting of all six nuclei together, versus $^{1}H_{\varepsilon 1}$ and $^{13}C_{\varepsilon 1}$ together, and versus $^{1}H_{\varepsilon 1}$ chemical shifts on their own, and for all residues, there were no significant differences in the pK_a values obtained.

Four of the nine His residues in hPRL fit well to the simplest model of a single, noninteracting pH titration site. Also, in all of the His to Ala mutations that were investigated, pH titrations for these residues overlapped well with the WT protein. Hence, we believe that H46, H138, H173, and H195 titrate in a classical manner, in a fashion independent from other residues. Representative, fitted titration curves for the $^{1}H_{\varepsilon 1}$ and $^{13}C_{\varepsilon 1}$ nuclei of H195 are shown at the top of Figure 6. Summarized in Table 4 are the fitted pK_a values for H46, H138, and H195 which fall within the typical range of 6.0−6.5, whereas the pK_a for H173 is unusually low (5.0). This residue is buried in the tertiary structure of hPRL. Protonation of H173 would result in the highly unfavorable burial of an uncompensated positive charge, most likely resulting in disruption of the local, favorable structural interactions to allow hydration of the charged residue. Therefore, the neutral state of H173 is effectively stabilized, evidenced by its more acidic pK_a.

In contrast to the four independently titrating residues mentioned above, our data suggest a strong interaction among H27, H30, and H180. First, inspection of Figure 5 shows how mutation of either H30 or H180 strongly perturbs the pH titration curve of the other. Note that an interaction was already suspected on the basis of the unusual pH-dependent trajectory of the H30 $^{15}N_{\delta 1}$ resonance in Figure 4. Similarly, titration curves for H27 and H30 in Figure 5 also show small, but significant, perturbations when the other is mutated; in contrast, H27 and H180 do not appear to have a significant direct interaction. Additional, independent evidence of these direct interactions can be derived from an analysis of their individual pH titration curves. In Table 1, we compare the results of simultaneous fitting the $^{1}H_{\varepsilon 1}$ titration curves for all three residues according to the thermodynamic model depicted in Figure 2, but considering four separate situations: (1) independent titration of all three residues, (2) linkage between H27 and H30 only, (3) linkage between H30 and H180 only, and (4) simultaneous linkage between both pairs of residues. At the bottom of Figure 6, best fit curves for the fully independent (1) and the fully interacting (4) models are compared to the experimental data.

Visually, it is evident from Figure 6 that the $^{1}H_{\varepsilon 1}$ titration curves for H30 and H180 do not fit well to the simplest model of independent protonation. The need for a more complex model to describe the titration of H27, H30, and H180 can be more rigorously supported by the use of the *F*-statistic. Calculation of *F*-statistics requires the residual sum-squared errors (SSEs) between the experimental data and their best fit values along with the degrees of freedom during fitting, which is derived from both the number of fitting parameters and the number of independent pieces of data. To more accurately describe the true degrees of freedom during the comparison of our three titration models, we have chosen to include only the $^{1}H_{\varepsilon 1}$ NMR chemical shift data,

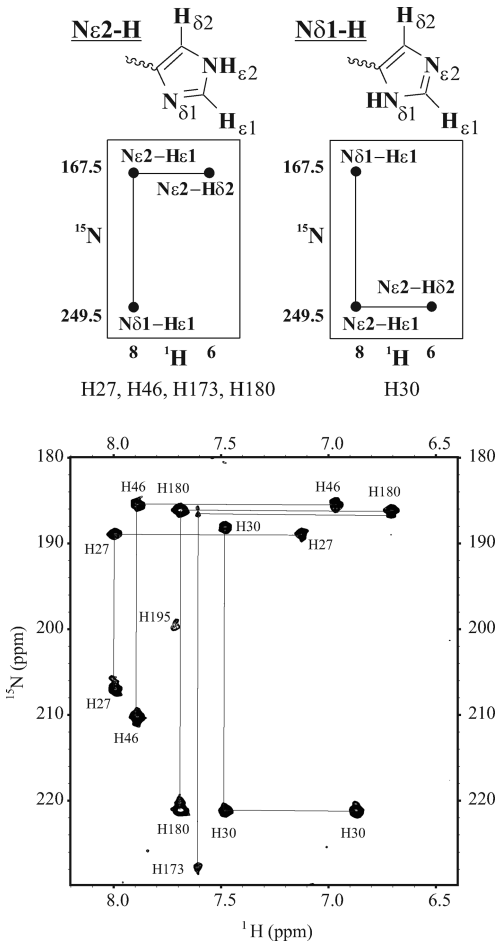

FIGURE 3: Schematic diagram (top) showing the nomenclature used to describe the two possible tautomeric states of the neutral imidazole ring of histidines, termed $N_{\varepsilon 2}$-H and $N_{\delta 1}$-H, and the expected pattern of long-range ($^2J_{NH}$) correlations in the $^1H-^{15}N$ HSQC NMR spectrum (adapted from ref (*33*)). $^1H-^{15}N$ HSQC spectrum (bottom) of [^{15}N]His-labeled hPRL in 25 mM potassium phosphate buffer (pH 7.5) and 25 mM NaCl recorded at 35 °C. Histidine cross-peak patterns are indicated for each residue. Tautomeric assignments for each residue are listed under the representative spectra. The tautomeric states of H57, H97, H138, and H195 have not been assigned.

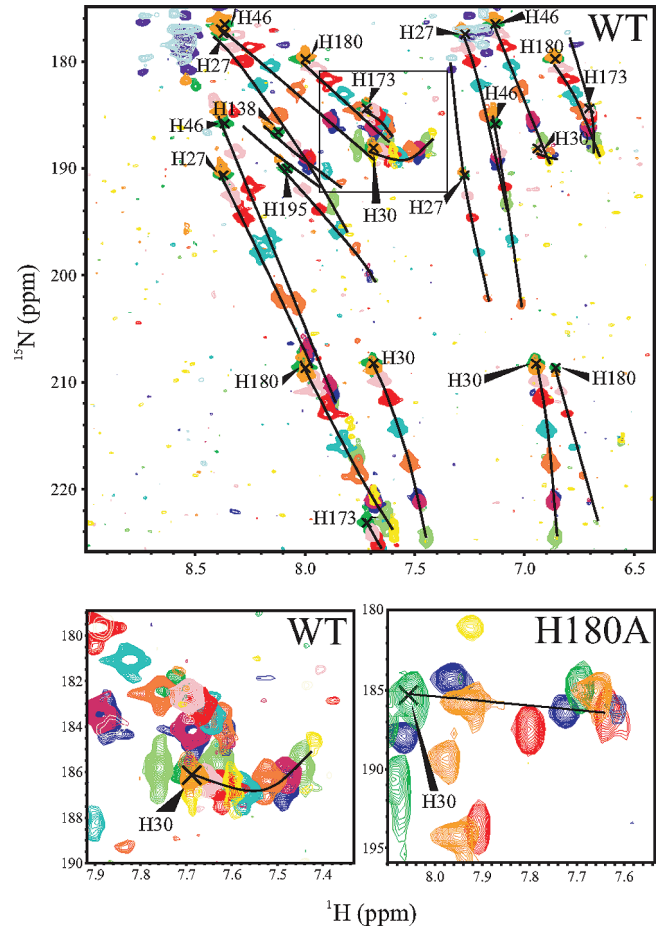

FIGURE 4: Overlaid $^1H-^{15}N$ HSQC NMR spectra of [^{15}N]His-labeled WT and H180A PRL from pH 4.5 to 8.0. The $^1H-^{15}N$ chemical shift changes with pH generally follow linear trajectories as illustrated by the black trace, with low-pH peaks at the start of the trajectories at the top left. Spectral expansions are shown at the bottom depicting the curved trajectory for the H30 $^1H_{\varepsilon 1}-^{15}N_{\delta 1}$ cross-peak in WT hPRL (left), which reverts to a linear trajectory in H180A hPRL (right).

as the data from this nucleus are the most complete for this triplet of residues. Elsewhere, we have simultaneously fit multiple NMR chemical shifts derived from a single sample (e.g., $^1H_{\varepsilon 1}$ and $^{13}C_{\varepsilon 1}$) to derive individual pK_a values for each residue. Although inclusion of multiple chemical shifts for each residue should not degrade the accuracy of the best fit value, it does distort estimation of the statistical errors by overestimating the number of truly independent pieces of data. In these experiments, the largest source of random error likely derives from the preparation of the individual NMR samples and, to a lesser degree, the separate acquisition of each NMR spectrum. These errors are contained equally in each of the chemical shift values acquired from each NMR spectrum collected on a single sample and, thus, cannot be considered truly independent measurements. This lack of independence is evidenced by a strong correlation between the residual errors (i.e., the difference between the experimental and fitted values) for each of the six nuclei in a single residue (not shown). By restricting our analysis to a single NMR chemical shift per residue, we are largely able to avoid this overestimation of the statistical degrees of freedom and be more confident in the applicability of the *F*-statistic in identifying and rejecting overly complex and statistically nonsignificant models. However, because we have chosen to globally fit the NMR chemical shifts for all three residues simultaneously (necessary for consideration of thermodynamic linkage between residues), we cannot avoid utilizing three independent variables from each NMR spectrum. Therefore, we have chosen to determine SSEs (Table 2) and *F*-statistics (Table 3) for each of the individual, dependent variables as well as their total. Neither approach is ideal, as the statistics for the isolated dependent variables ignore the compromises occurring during global fitting of the three residues simultaneously and, as well, the statistics for the overall (total) fit likely overestimate the number of independent data points.

Beginning at the top of Table 3, *F*-statistics for the isolated H27 $^1H_{\varepsilon 1}$-dependent variable support the inclusion of thermodynamic linkage between H27 and H30, despite the small visual difference between the fitted curves for H27 in Figure 4. Note that the additional inclusion of linkage between H30 and H180 did not improve the fit for H27 when considered on its own, which should be expected. Similarly, when considering only the quality of fit for the H180 $^1H_{\varepsilon 1}$-dependent variable, the *F*-statistics clearly support the

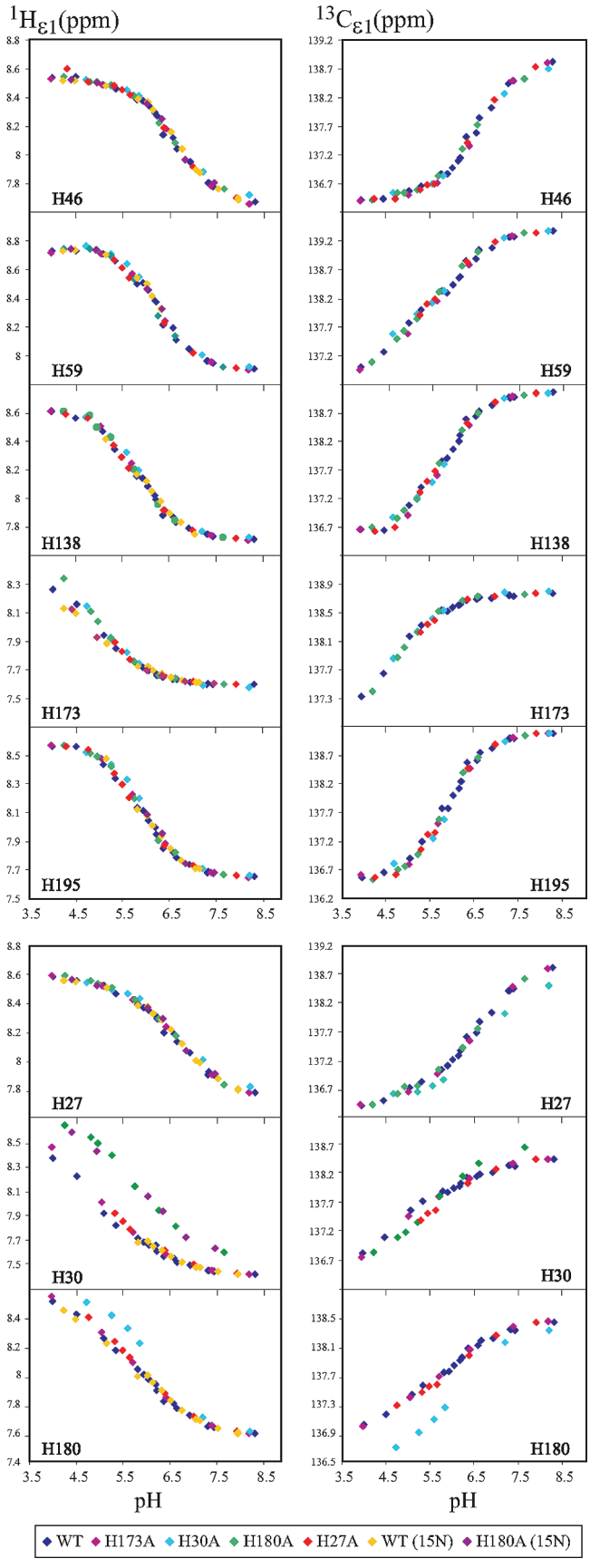

FIGURE 5: $^1H_{\varepsilon1}$ and $^{13}C_{\varepsilon1}$ NMR chemical shifts plotted against solution pH for eight of the nine His residues in hPRL. Titrations are superposed for both WT and multiple His to Ala mutants of hPRL.

presence of negative cooperativity between H30 and H180, but consideration of linkage between H27 and H30 does not

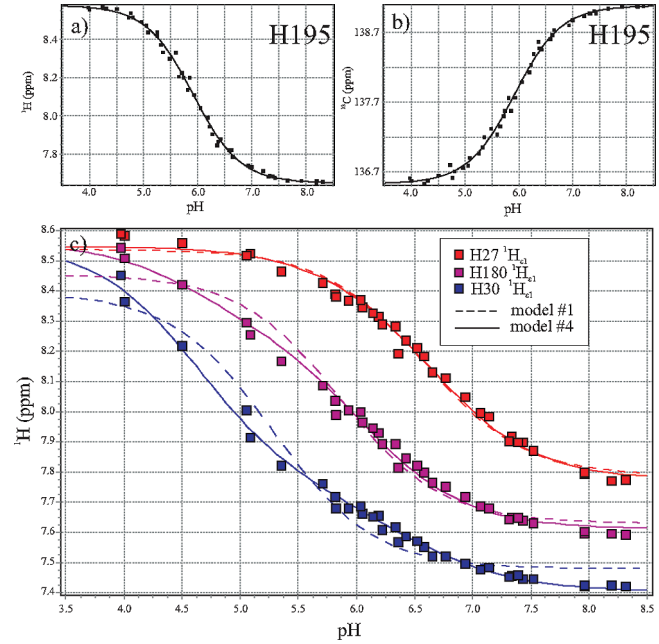

FIGURE 6: Experimental NMR chemical shifts and best fit theoretical curves for histidine imidazole ring nuclei in WT hPRL as a function of pH. Panels a and b display $^1H_{\varepsilon1}$ and $^{13}C_{\varepsilon1}$ NMR chemical shifts, respectively, for H195 fitted to a classic, noninteracting model of protonation. In panel c, $^1H_{\varepsilon1}$ chemical shifts for residues H30 (blue), H180 (mauve), and H27 (red) are shown with the best fit curves for both the fully independent model (dashed line, $c_{27,180} = c_{30,180} = 1$, model 1 in Table 1) and the fully interacting model (solid line, $c_{27,30} = 0.42$ and $c_{30,180} = 0.14$, model 4 in Table 1) for each residue, colored to match the experimental data.

Table 4: Summary of the Best Fit Binding Parameters and the Corresponding 95% Confidence Intervals

	best fit	95% confidence interval
H46 pK_a	6.56	6.51−6.58
H59 pK_a	5.84	5.71−5.97
H138 pK_a	5.82	5.77−5.87
H173 pK_a	4.99	4.91−5.07
H195 pK_a	5.91	5.87−5.96
H27 pK_a	6.64	6.49−6.79
H30 pK_a	6.00	5.67−6.33
H180 pK_a	5.96	5.83−6.09
$c_{27,30}$	0.42	0.03−0.82
$c_{30,180}$	0.14	0.02−0.27

improve agreement for H180. The situation for the H30 $^1H_{\varepsilon1}$-dependent variable is more complex. The quality of fit for H30 is improved in all cases by the addition of thermodynamic linkage between either pairs of residues (see Table 2), and the corresponding *F*-statistics are significant at a probability >95% for all comparisons except for one (see Table 3). Lastly, when all of the experimental data are considered together, inclusion of both thermodynamic linkage parameters greatly improves the quality of the fit and the corresponding *F*-statistics are highly significant in all cases, although the degree of statistical confidence is likely overestimated by the lack of complete independence between the data for each residue. Regardless, when all of the evidence is considered in aggregate, the existence of negative cooperativity between H27 and H30 and also between H30 and H180 is clear. The quality of the fit for H27 and H30 depends on their linkage, and similarly, the quality of fit for H30 and H180 depends on their linkage. This statistical analysis is supported by the deviation in the NMR chemical

shift titration curves for each residue in the His to Ala mutants shown in Figure 5.

We present in Table 4 our current, best assessment of the thermodynamic parameters describing the protonation reactions of eight of the nine His residues in hPRL. Note that although there can be no doubt about the existence of negative cooperativity among residues H27, H30, and H180, we cannot define the individual cooperativity constants with precision. In our various attempts to globally fit the selected NMR data to various models, these constants displayed the greatest variability in their best fit values. However, interestingly, their product ($c_{27,30}c_{30,180}$) remained roughly constrained to the order of ~0.1. This conservation was likely required to properly account for the reduced slope of the transition seen in the H30 $^1H_{\varepsilon 1}$ titration curve compared to the noncooperative case. Although our data appear to lack statistical power to precisely define their individual values, there is sufficient evidence to conclude that the negative cooperativity between H30 and H180 is stronger than that between H27 and H30. First, the H30 $^{15}N_{\delta 1}$ NMR chemical shift in Figure 4 appears to depend on titration of both the H30 and H180 imidazole rings. Second, a more dramatic change is seen in the titration curves of both H30 and H180 when either is mutated as compared to H27 and H30. This conclusion is further supported by the closer relationship between H30 and H180 in the tertiary structure of hPRL compared to that of H27 and H30. Therefore, we have chosen to include the best fit values for these cooperativity constants in Table 4 as their relative magnitudes are in agreement with our assessment. However, uncertainty in their precise values is appropriately reflected in their relatively large 95% confidence limits.

Throughout the description given above, we have purposely avoided discussion of the results for residues H59 and H97. In all of the above-described NMR spectra of WT hPRL, NMR signals for the imidazole ring of H97 are either extremely weak or unobservable. Interestingly, when H59 was mutated to Ala (to confirm its assignment), a new strong NMR signal was observed, which was assigned as belonging to H97. Although not in direct contact, H59 and H97 are nearby structurally, and both are part of a small cluster of aromatic residues between the two long loops and the second and fourth helices. The most likely explanation for our results is that in WT hPRL the H97 imidazole NMR signals undergo chemical exchange on a time scale similar to their difference in NMR chemical shifts, most likely due to conformational mobility within this aromatic cluster. Mutation of H59 to Ala would be expected to structurally loosen these interactions and, thereby, increase the mobility of H97 to a faster exchange regime where it becomes observable. We also notice that the titration curve for H59 displays slight, systematic deviations from a model of independent titration similar to that of H30 and H180. We are currently investigating the structural and thermodynamic linkage between H59 and H97, which will be detailed in a future publication.

Contribution of Selected Histidines to Global Unfolding of hPRL. The individual contribution of each histidine within the interacting triplet to the global stability of hPRL was investigated using chemical denaturation. Figure 7 plots normalized, intrinsic Trp fluorescence across a wide range of urea concentrations for WT, H27A, H30A, and H180A hPRL. Approximately two-state global unfolding of the proteins is indicated by the sudden and sharp transitions between nativelike and denatured protein fluorescence. Shifts in the global unfolding transitions to lower or higher urea concentrations indicate decreases or increases in the global unfolding free energies (ΔG_{unf}), respectively. The experimental data have been fit to a theoretical description of unfolding as previously described (*18*) to derive quantitative descriptions of $[urea]_{mid}$, the urea concentration at the midpoint of the transition, and the ΔG_{unf} for each protein. The data clearly indicate that the presence of each individual imidazole ring for residues H27, H30, and H180 is overall destabilizing with respect to protein folding.

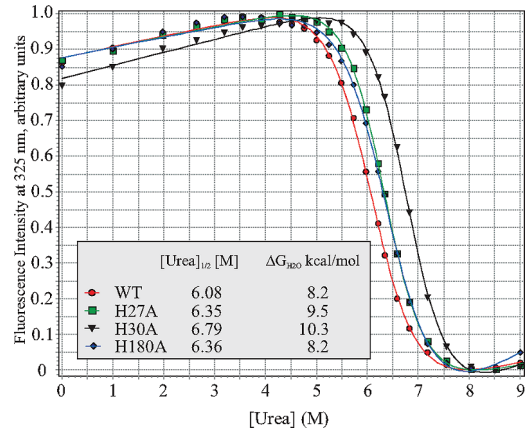

FIGURE 7: Chemical denaturation curves of WT, H27A, H30A, and H180A hPRL for a comparison of their global stabilities. Normalized, intrinsic Trp fluorescence is plotted as a function of urea concentration, and the data are fitted to theoretical curves, from which are derived the displayed $[urea]_{med}$ and ΔG_{unf} values.

DISCUSSION

Proteins often display pH dependence with respect to their structural stability and functional behavior. Such pH dependence is ultimately mediated by the thermodynamics of protonation reactions of ionizable groups, which are located primarily in the side chains of Asp, Glu, His, Arg, and Lys residues. The pH dependence of any equilibrium between protein structural states (and thus functional states) can be completely described by detailing all the changes in protonation equilibrium constants (i.e., the pK_a values) for all the individual ionizable groups. NMR spectroscopy is uniquely suited to describing site-specific protonation and has been routinely utilized to derive residue-specific pK_a values (*39*–*49*), during which the identification of thermodynamic linkage between protonation sites is not uncommon. We recently discovered dramatic pH dependence to both the structural stability and receptor binding affinity of hPRL, over the relatively narrow physiologic pH range of 6−8 (*18*). As the initial step to detailing the molecular basis of this pH dependence, we have analyzed the site-specific (or microscopic) titration curves for eight of the nine His residues in hPRL. In doing so, we describe a novel approach for combining a statistical analysis of NMR titration curves with site-directed mutagenesis in identifying thermodynamic linkage, or cooperativity, between the protonation reactions of individual residues.

The protonation equilibrium constants (pK_a values) for the histidines in hPRL all fall in a relatively typical range from 5.8 to 6.6, with the exception of H173, whose unusually

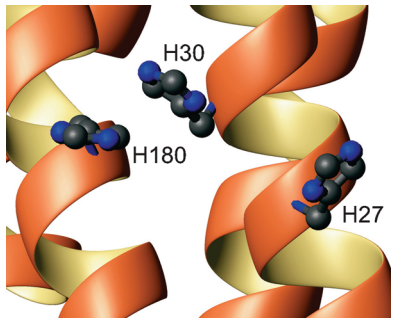

FIGURE 8: Positions of the H27, H30, and H180 imidazole rings in the X-ray crystallographic structure of a hPRL variant (PDB entry 2Q98).

acidic pK_a of 5.0 is likely the result of the complete burial of its imidazole ring. The unusual and somewhat novel finding is the presence of thermodynamic linkage between the protonation reactions of H27, H30, and H180, corresponding to an overall perturbation in the free energy of protonation of approximately 1.4 kcal/mol. We considered the possibility of hydrogen bonding between these coupled imidazole rings, but this was not supported by their positioning in either the NMR (*29*) or X-ray (*28*) structure of hPRL. As shown in Figure 8, H27 and H30 are not close enough to support hydrogen bonding (>3 Å) and H30 and H180 are stacked vertically in a staggered manner, consistent with favorable aromatic stacking interactions. Therefore, on the basis of this positioning, it appears more likely for the negative cooperativity between protonation reactions to be governed primarily by unfavorable electrostatics or, possibly, interference with aromatic stacking.

The thermodynamic interactions among H27, H30, and H180 described here are likely to contribute to the biological function of hPRL, based on both their presumed structural location within the high-affinity receptor binding site (*29*) and an evolutionary argument regarding their unfavorable contribution to protein stability. First, although the structure of hPRL bound to its receptor has not been described, the related protein hGH also binds to the hPRL receptor (but only in the presence of Zn^{2+}), and a high-resolution structure of this complex has been reported (*50*). H27 and H30 from hPRL are conserved in hGH. Structurally, these homologous residues are located within the binding interface and directly coordinate the Zn^{2+} cation required for receptor recognition. H180 is homologous to an Asp in hGH that is also located within the interface but does not interact directly with the Zn^{2+} cation. Site-specific mutation of H27, H30, or H180 has been shown to decrease either the receptor binding affinity or the mitogenic effects of hPRL (*51*), further supporting their expected location within the high-affinity receptor binding site. We also report here that single-site mutation of either H27, H30, or H180 in hPRL stabilizes the folded protein relative to its chemically denatured state. This is an unusual finding as a majority of amino acids in proteins appear to be evolutionarily optimized toward their contribution to global stability (*52*). Conformational strain associated with conserved residues, such as that seen here, is often an indicator of functional importance. Although the current results do not clearly define the structural basis of the previously reported pH-dependent behavior (*18*), they do form a foundation for ongoing studies of the contribution of specific His residues to the structural stability and receptor binding properties of hPRL. In the future, we hope that by directly measuring site-specific changes in pK_a values associated with receptor binding and protein unfolding, we can realize a better understanding of the biophysical basis of hPRL's pH-dependent behavior.

ACKNOWLEDGMENT

We thank Drs. Jay Emerson and John Hartigan in the Department of Statistics, Yale University, for useful discussions.

SUPPORTING INFORMATION AVAILABLE

^1H, ^{13}C, and ^{15}N chemical shifts for WT hPRL and H27A, H30A, and H180A hPRL mutants from the $^1H-^{13}C$ HSQC and $^1H-^{15}N$ HSQC NMR spectra. This material is available free of charge via the Internet at http://pubs.acs.org.

REFERENCES

1. Goffin, V., Binart, N., Touraine, P., and Kelly, P. A. (2002) Prolactin: The new biology of an old hormone. *Annu. Rev. Physiol. 64*, 47–67.
2. Wells, J. A., and de Vos, A. M. (1996) Hematopoietic receptor complexes. *Annu. Rev. Biochem. 65*, 609–634.
3. Ben-Jonathan, N., Mershon, J. L., Allen, D. L., and Steinmetz, R. W. (1996) Extrapituitary prolactin: Distribution, regulation, functions, and clinical aspects. *Endocr. Rev. 17*, 639–669.
4. Ben-Jonathan, N., Liby, K., McFarland, M., and Zinger, M. (2002) Prolactin as an autocrine/paracrine growth factor in human cancer. *Trends Endocrinol. Metab. 13*, 245–250.
5. Clevenger, C. V., Furth, P. A., Hankinson, S. E., and Schuler, L. A. (2003) The role of prolactin in mammary carcinoma. *Endocr. Rev. 24*, 1–27.
6. Goffin, V., Touraine, P., Pichard, C., Bernichtein, S., and Kelly, P. A. (1999) Should prolactin be reconsidered as a therapeutic target in human breast cancer? *Mol. Cell. Endocrinol. 151*, 79–87.
7. Leav, I., Merk, F. B., Lee, K. F., Loda, M., Mandoki, M., McNeal, J. E., and Ho, S. M. (1999) Prolactin receptor expression in the developing human prostate and in hyperplastic, dysplastic, and neoplastic lesions. *Am. J. Pathol. 154*, 863–870.
8. Xu, X., Kreye, E., Kuo, C. B., and Walker, A. M. (2001) A molecular mimic of phosphorylated prolactin markedly reduced tumor incidence and size when DU145 human prostate cancer cells were grown in nude mice. *Cancer Res. 61*, 6098–6104.
9. Bernichtein, S., Kinet, S., Jeay, S., Llovera, M., Madern, D., Martial, J. A., Kelly, P. A., and Goffin, V. (2001) S179D-human PRL, a pseudophosphorylated human PRL analog, is an agonist and not an antagonist. *Endocrinology 142*, 3950–3963.
10. Xu, X., Wu, W., Williams, V., Khong, A., Chen, Y. H., Deng, C., and Walker, A. M. (2003) Opposite effects of unmodified prolactin and a molecular mimic of phosphorylated prolactin on morphology and the expression of prostate specific genes in the normal rat prostate. *Prostate 54*, 25–33.
11. Ueda, E., Ozerdem, U., Chen, Y. H., Yao, M., Huang, K. T., Sun, H., Martins-Green, M., Bartolini, P., and Walker, A. M. (2006) A molecular mimic demonstrates that phosphorylated human prolactin is a potent anti-angiogenic hormone. *Endocr.-Relat. Cancer 13*, 95–111.
12. Maciejewski, P. M., Peterson, F. C., Anderson, P. J., and Brooks, C. L. (1995) Mutation of serine 90 to glutamic acid mimics phosphorylation of bovine prolactin. *J. Biol. Chem. 270*, 27661–27665.
13. Schenck, E. J., Canfield, J. M., and Brooks, C. L. (2003) Functional relationship of serine 90 phosphorylation and the surrounding putative salt bridge in bovine prolactin. *Mol. Cell. Endocrinol. 204*, 117–125.
14. Aranda, J., Rivera, J. C., Jeziorski, M. C., Riesgo-Escovar, J., Nava, G., Lopez-Barrera, F., Quiroz-Mercado, H., Berger, P., Martinez de la Escalera, G., and Clapp, C. (2005) Prolactins are natural inhibitors of angiogenesis in the retina. *Invest. Ophthalmol. Visual Sci. 46*, 2947–2953.
15. Piwnica, D., Touraine, P., Struman, I., Tabruyn, S., Bolbach, G., Clapp, C., Martial, J. A., Kelly, P. A., and Goffin, V. (2004)

Cathepsin D processes human prolactin into multiple 16K-like N-terminal fragments: Study of their antiangiogenic properties and physiological relevance. *Mol. Endocrinol. 18*, 2522–2542.
16. Corbacho, A. M., Nava, G., Eiserich, J. P., Noris, G., Macotela, Y., Struman, I., Martinez de la Escalera, G., Freeman, B. A., and Clapp, C. (2000) Proteolytic cleavage confers nitric oxide synthase inducing activity upon prolactin. *J. Biol. Chem. 275*, 13183–13186.
17. Clapp, C., Martial, J. A., Guzman, R. C., Rentierdelrue, F., and Weiner, R. I. (1993) The 16-Kilodalton N-Terminal Fragment of Human Prolactin Is a Potent Inhibitor of Angiogenesis. *Endocrinology 133*, 1292–1299.
18. Keeler, C., Jablonski, E. M., Albert, Y. B., Taylor, B. D., Myszka, D. G., Clevenger, C. V., and Hodsdon, M. E. (2007) The kinetics of binding human prolactin, but not growth hormone, to the prolactin receptor vary over a physiologic pH range. *Biochemistry 46*, 2398–2410.
19. Dannies, P. S. (2002) Mechanisms for storage of prolactin and growth hormone in secretory granules. *Mol. Genet. Metab. 76*, 6–13.
20. Sankoorikal, B. J., Zhu, Y. L., Hodsdon, M. E., Lolis, E., and Dannies, P. S. (2002) Aggregation of human wild-type and H27A-prolactin in cells and in solution: Roles of Zn^{2+}, Cu^{2+}, and pH. *Endocrinology 143*, 1302–1309.
21. Hilfiker-Kleiner, D., Kaminski, K., Podewski, E., Bonda, T., Schaefer, A., Sliwa, K., Forster, O., Quint, A., Landmesser, U., Doerries, C., Luchtefeld, M., Poli, V., Schneider, M. D., Balligand, J. L., Desjardins, F., Ansari, A., Struman, I., Nguyen, N. Q., Zschemisch, N. H., Klein, G., Heusch, G., Schulz, R., Hilfiker, A., and Drexler, H. (2007) A cathepsin D-cleaved 16 kDa form of prolactin mediates postpartum cardiomyopathy. *Cell 128*, 589–600.
22. Leinwand, L. A. (2007) Molecular events underlying pregnancy-induced cardiomyopathy. *Cell 128*, 437–438.
23. Piwnica, D., Fernandez, I., Binart, N., Touraine, P., Kelly, P. A., and Goffin, V. (2006) A new mechanism for prolactin processing into 16K PRL by secreted cathepsin D. *Mol. Endocrinol. 20*, 3263–3278.
24. Clapp, C., Gonzalez, C., Macotela, Y., Aranda, J., Rivera, J. C., Garcia, C., Guzman, J., Zamorano, M., Vega, C., Martin, C., Jeziorski, M. C., and Martinez de la Escalera, G. (2006) Vasoinhibins: A family of N-terminal prolactin fragments that inhibit angiogenesis and vascular function. *Front. Horm. Res. 35*, 64–73.
25. Lkhider, M., Castino, R., Bouguyon, E., Isidoro, C., and Ollivier-Bousquet, M. (2004) Cathepsin D released by lactating rat mammary epithelial cells is involved in prolactin cleavage under physiological conditions. *J. Cell Sci. 117*, 5155–5164.
26. Gerweck, L. E. (2000) The pH difference between tumor and normal tissue offers a tumor specific target for the treatment of cancer. *Drug Resist. Updates 3*, 49–50.
27. Brooks, D. J., Fresco, J. R., Lesk, A. M., and Singh, M. (2002) Evolution of amino acid frequencies in proteins over deep time: Inferred order of introduction of amino acids into the genetic code. *Mol. Biol. Evol. 19*, 1645–1655.
28. Jomain, J. B., Tallet, E., Broutin, I., Hoos, S., van, A. J., Ducruix, A., Kelly, P. A., Kragelund, B. B., England, P., and Goffin, V. (2007) Structural and thermodynamical bases for the design of pure prolactin receptor antagonists. X-ray structure of Del1-9G129R-hPRL. *J. Biol. Chem. 282*, 33118–33131.
29. Teilum, K., Hoch, J. C., Goffin, V., Kinet, S., Martial, J. A., and Kragelund, B. B. (2005) Solution structure of human prolactin. *J. Mol. Biol. 351*, 810–823.
30. Keeler, C., Dannies, P. S., and Hodsdon, M. E. (2003) The tertiary structure and backbone dynamics of human prolactin. *J. Mol. Biol. 328*, 1105–1121.
31. Waugh, D. S. (1996) Genetic tools for selective labeling of proteins with α-^{15}N-amino acids. *J. Biomol. NMR 8*, 184–192.
32. Peterson, F. C., Gordon, N. C., and Gettins, P. G. (2001) High-level bacterial expression and ^{15}N-alanine-labeling of bovine trypsin. Application to the study of trypsin-inhibitor complexes and trypsinogen activation by NMR spectroscopy. *Biochemistry 40*, 6275–6283.
33. Pelton, J. G., Torchia, D. A., Meadow, N. D., and Roseman, S. (1993) Tautomeric states of the active-site histidines of phosphorylated and unphosphorylated IIIGlc, a signal-transducing protein from *Escherichia coli*, using two-dimensional heteronuclear NMR techniques. *Protein Sci. 2*, 543–558.
34. Delaglio, F., Grzesiek, S., Vuister, G. W., Zhu, G., Pfeifer, J., and Bax, A. (1995) Nmrpipe: A Multidimensional Spectral Processing System Based on Unix Pipes. *J. Biomol. NMR 6*, 277–293.
35. Kneller, D. G., and Goddard, T. D. (1997) SPARKY, University of California, San Francisco.
36. Cavanagh, J. (1996)Referencing. In *Protein NMR Spectroscopy: Principles and Practice*, pp 175−176, Academic Press, San Diego.
37. Gill, S. J., Richey, B., Bishop, G., and Wyman, J. (1985) Generalized binding phenomena in an allosteric macromolecule. *Biophys. Chem. 21*, 1–14.
38. Bachovchin, W. W. (1986) ^{15}N NMR spectroscopy of hydrogen-bonding interactions in the active site of serine proteases: Evidence for a moving histidine mechanism. *Biochemistry 25*, 7751–7759.
39. Andre, I., Linse, S., and Mulder, F. A. (2007) Residue-specific pKa determination of lysine and arginine side chains by indirect ^{15}N and ^{13}C NMR spectroscopy: Application to apo calmodulin. *J. Am. Chem. Soc. 129*, 15805–15813.
40. Chivers, P. T., Prehoda, K. E., Volkman, B. F., Kim, B. M., Markley, J. L., and Raines, R. T. (1997) Microscopic pKa values of *Escherichia coli* thioredoxin. *Biochemistry 36*, 14985–14991.
41. Gao, G., DeRose, E. F., Kirby, T. W., and London, R. E. (2006) NMR determination of lysine pKa values in the Pol λ lyase domain: Mechanistic implications. *Biochemistry 45*, 1785–1794.
42. Joshi, M. D., Hedberg, A., and McIntosh, L. P. (1997) Complete measurement of the pKa values of the carboxyl and imidazole groups in *Bacillus circulans* xylanase. *Protein Sci. 6*, 2667–2670.
43. Kesvatera, T., Jonsson, B., Thulin, E., and Linse, S. (1996) Measurement and modelling of sequence-specific pKa values of lysine residues in calbindin D9k. *J. Mol. Biol. 259*, 828–839.
44. Khare, D., Alexander, P., Antosiewicz, J., Bryan, P., Gilson, M., and Orban, J. (1997) pKa measurements from nuclear magnetic resonance for the B1 and B2 immunoglobulin G-binding domains of protein G: Comparison with calculated values for nuclear magnetic resonance and X-ray structures. *Biochemistry 36*, 3580–3589.
45. Lindman, S., Linse, S., Mulder, F. A., and Andre, I. (2006) Electrostatic contributions to residue-specific protonation equilibria and proton binding capacitance for a small protein. *Biochemistry 45*, 13993–14002.
46. McIntosh, L. P., Hand, G., Johnson, P. E., Joshi, M. D., Korner, M., Plesniak, L. A., Ziser, L., Wakarchuk, W. W., and Withers, S. G. (1996) The pKa of the general acid/base carboxyl group of a glycosidase cycles during catalysis: A ^{13}C-NMR study of *Bacillus circulans* xylanase. *Biochemistry 35*, 9958–9966.
47. Oliveberg, M., Arcus, V. L., and Fersht, A. R. (1995) pKa values of carboxyl groups in the native and denatured states of barnase: The pKa values of the denatured state are on average 0.4 units lower than those of model compounds. *Biochemistry 34*, 9424–9433.
48. Schubert, M., Poon, D. K., Wicki, J., Tarling, C. A., Kwan, E. M., Nielsen, J. E., Withers, S. G., and McIntosh, L. P. (2007) Probing electrostatic interactions along the reaction pathway of a glycoside hydrolase: Histidine characterization by NMR spectroscopy. *Biochemistry 46*, 7383–7395.
49. Tan, Y. J., Oliveberg, M., Davis, B., and Fersht, A. R. (1995) Perturbed pKa-values in the denatured states of proteins. *J. Mol. Biol. 254*, 980–992.
50. Somers, W., Ultsch, M., DeVos, A. M., and Kossiakoff, A. A. (1994) The X-Ray Structure of a Growth-Hormone Prolactin Receptor Complex. *Nature 372*, 478–481.
51. Goffin, V., Shiverick, K. T., Kelly, P. A., and Martial, J. A. (1996) Sequence-function relationships within the expanding family of prolactin, growth hormone, placental lactogen, and related proteins in mammals. *Endocr. Rev. 17*, 385–410.
52. Richards, F. M. (1997) Protein stability: Still an unsolved problem. *Cell. Mol. Life Sci. 53*, 790–802.

BI800444T